Hindawi
Advances in Civil Engineering
Volume 2019, Article ID 5917380, 12 pages
https://doi.org/10.1155/2019/5917380

Research Article

Quasistatic Cyclic Tests and Finite Element Analysis of Low-Aspect Ratio Double Steel Concrete Composite Walls

Kaize Ma, Yudong Ma, and Boquan Liu

Department of Civil Engineering, Chang'an University, Xi'an, China

Correspondence should be addressed to Kaize Ma; makaize@chd.edu.cn

Received 16 October 2018; Revised 14 January 2019; Accepted 11 February 2019; Published 9 April 2019

Academic Editor: Lukasz Sadowski

An innovative double steel concrete (DSC) composite wall was developed to enhance constructability and lateral load resistance of buildings. Three low-aspect ratio DSC composite walls were constructed and tested to study the shear behavior. Under different testing parameters, the failure modes, hysteresis behavior, lateral load resisting capacity, deformation, and energy dissipation of the composite walls were observed. The results showed that all specimens failed in shear behavior with steel plate buckling and concrete compressive crushing. The pinching behavior was obvious for hysteresis loops of composite walls. Moreover, the lateral load resisting capacity and deformation were significantly affected with axial compression ratio and steel ratio. Beyond that, the ductility coefficients of specimens reached 3.30. The finite element (FE) method was performed to analyze the failure process of the specimens with cyclic analysis. The concrete damage plastic model (CPDM) was selected to simulate the damage progress of concrete. Validation of the FE models against the experimental results showed good agreement.

1. Introduction

Shear wall is one of the most common lateral resistance members for high-rise buildings, which can improve the lateral stiffness and lateral load resisting capacity of the structure. Reinforced concrete (RC) shear wall, as a common shear wall, is widely adopted, and the experimental studies on RC shear walls have already been conducted. Ricci et al. tested cellular structures composed of cast in situ sandwich squat concrete walls. The results showed that the seismic performances of the tested sandwich panels are comparable with those of common R/C panels and can withstand horizontal load, at large interstorey drift, also to vertical load-carrying capacity [1, 2].

With the improvement of requirement on higher strength, faster construction, and cost effectiveness, conventional RC walls are no longer applied to all structures. Double steel concrete (DSC) composite wall is a new form of the shear wall [3, 4], which could solve the above problems. Two steel plates are positioned outside the wall, and concrete was poured between the steel plates. Steel studs provide composite action between the concrete and steel plates. The steel plate and concrete are constrained with each other, thereby increasing the stiffness, lateral load resisting capacity, and deformation of composite walls.

Considerable efforts have been made to investigate the behavior of DSC composite walls. Prabha et al. [5] analyzed the effect of constraint on DSC composite wall on the axial capacity. Zhang et al. [6] and Hu et al. [7] analyzed the effects of shear connector on DSC walls, and the calculation method of ultimate curvature was advised. Emori et al. [8] tested a new DSC composite wall structural system under compressive and shear loading. The results indicated that the wall had excellent strength and ductility. And the best width thickness ratio of surface steel plate was 100. Clubley et al. [9, 10] investigated the shear capacity of steel concrete composite panels by testing and numerical modelling. The results showed that a sufficient shear capacity of bi-steel system is demonstrated under push-out load, and the parameters such as plate spacing, connector spacing, and shear connector diameter were the main factors affecting shear capacity. Wright et al. [11, 12] researched the behavior of the composite wall made of steel plate with infill

of normal concrete and lightweight concrete. Eom et al. [13] tested five slender double skin composite walls under cyclic loading for the study of the seismic behavior of the walls. They found that the walls had excellent lateral load resisting capacities, and the strengthening methods of wall base were the main factor affecting the ductility. Nie et al. [14] tested twelve DSC composite walls to evaluate the seismic behavior. The results showed that the energy dissipation ability of all specimens was good, and the ultimate drift ratios ranged from 1/76 to 1/54. And on the basis of section analysis method, a strength prediction approach was also proposed. Ji et al. [15] researched the seismic behavior of the steel tube-double steel plate-concrete composite wall. The results indicated that specimens failed in a flexural mode, and the deformation and energy dissipation capacities were significantly affected by the extent of the steel tube boundary element. The seismic behavior of double steel plate high-strength concrete composite walls was evaluated by Chen at al. [16]. What is found in the test is that the strength and deformation capacity of wall specimens were excellent, compared with conventional high-strength concrete walls. And the strength and deformation capacity were mainly influenced by the axial compression ratio. Alzeni et al. [17] researched the seismic performance of DSC walls with and without boundary elements. They found that the theoretical plastic moment capacity of all tested walls was surpassed, and a stable ductile behavior up to 3% drift was also exhibited. The seismic performance of DSC composite walls was analyzed deterministically using the finite element analysis (FEA). A finite element model of flexure-critical composite shear walls in LS-DYNA was developed by Siamak et al. [18], which showed good consistency with test results in nonlinear cyclic response. Polat et al. [19] established the finite element model of DSC composite walls and verified its correctness. Meanwhile, some aspects of wall behavior, which is valuable for the design of composite walls, were provided.

Cyclic test was presented in this study which has some principle objectives summarized as follows: (1) to research some representative seismic results of the DSC composite wall such as lateral load resisting capacity, deformation capacity, and energy dissipation capacity and (2) to analyze the failure process of DSC composite walls by establishing a reliable numerical model.

2. Experimental Detail

2.1. Design of Experimental Specimens. The specimens represented the lower storeys of shear walls in the high-rise buildings and had dominant shear behavior. The testing limitations (height and maximum loads) also affected the aspect ratio and dimensions of specimens. Specimens are designed and fabricated in 1/4 scale. The configurations and dimensions of test specimens and steel details provided for the specimens are shown in Figure 1 and Table 1. Three test specimens were conducted during the experimental study labelled from DSCW-1 to DSCW-3. The experimental parameters were axial compression ratio and steel ratio. The cross-sectional size was 700 mm × 100 mm, and each panel was used for both boundary elements. Steel studs were welded on steel plate, which provided composite action between the concrete and steel plate. The foundation beam was designed to be a steel concrete composite beam according to test requirement. The thickness of steel plate was 10 mm. To achieve full anchorage, the double steel concrete wall was penetrated into foundation beam. The foundation beam is cast concrete with the double steel concrete wall. The calculated height of composite walls was 700 mm, and the aspect ratio was 1.0 for all specimens.

The concrete axial compressive strength values were obtained on the day of testing. The prism compressive strength (f_u) and cylinder compressive strength (f_c') of concrete was 62.9 Mpa and 53.9 Mpa, which were obtained from the mechanical test. The prism had a square cross section of 150 mm and a length of 300 mm, and the cylinder had a diameter of 150 mm and a length of 300 mm. The yield and ultimate strengths of steel plate with thickness of 2.5 mm and 3 mm were determined with tensile tests of steel samples and were found as 323 MPa to 430 MPa and 334 MPa to 457 MPa, respectively.

2.2. Test Setup and Instrumentation. The test setup employed for the specimens is shown in Figure 2. Steel concrete composite beam was cast on top of specimen to distribute the lateral loads. A testing frame of steel was used to carry out the quasistatic tests in this research program. Steel bolts were used to connect the foundation beams and the reaction floor, ensuring they were in a hole. Beyond that, the load was applied horizontally; the actuator was bolted to the top beams. The device of a sliding cart was exploited to make the jack move in the vertical direction. The data of cyclic loading was recorded by a MTS hydraulic jack whose scale was 1000 kN. And the lateral loading point was chosen at the distance of 700 mm above the foundation. During the experiment, all of the specimens were subjected to same loading history in the identical condition. In order to ensure the constant in vertical load, the hydraulic jack with a sensor was applied, which made the value of that to be monitored, and some adjustment could be applied if a large fluctuation happened.

All the specimens were tested under lateral quasistatic cyclic displacement to simulate seismically induced displacement demands. Each displacement step was repeated twice prior to moving to the next cycle. The displacement loading history of the specimens is shown in Figure 3. Firstly, the displacement increment was applied in 0.1% drift. As the lateral drift reached 0.6% drift, the displacement increment of 0.2% drift was used to control the loading cycles. As the composite wall load decreased to 85% of maximum load, the tests stopped or the composite wall did not bear the axial compression load, and the tests stopped. To record the displacements of the experimental specimens, the linear variable displacement transducers (LVDTs) were applied. To gauge the yield of steel plate, the strain gauges (G) were applied and attached at various

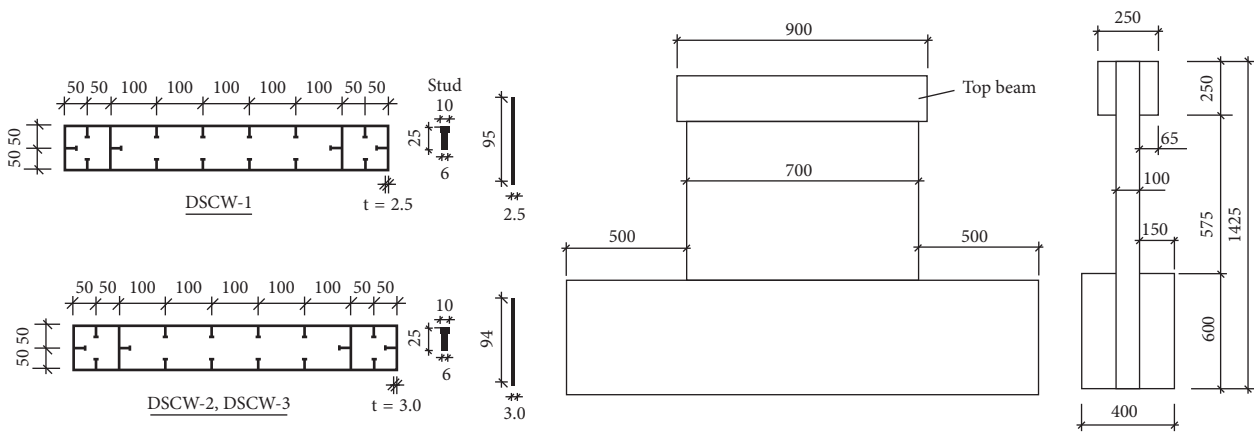

Figure 1: Geometries of DSC composite walls (dimensions in mm).

Table 1: Parameters of test specimens.

Specimens	$H \times h \times b$/mm	λ	n	N/kN	t/mm	Steel ratio (%)
DSCW-1	700 × 700 × 100	1.0	0.1	472	2.5	6.4
DSCW-2	700 × 700 × 100	1.0	0.1	493	3.0	7.7
DSCW-3	700 × 700 × 100	1.0	0.2	982	3.0	7.7

Note. H is the calculated height of the specimen, h is the height of the specimen cross section, b is the width of the specimen cross section, λ is the shear span ratio, n is the axial compression load ratio, N is the axial compression load, and t is the thickness of the steel plate.

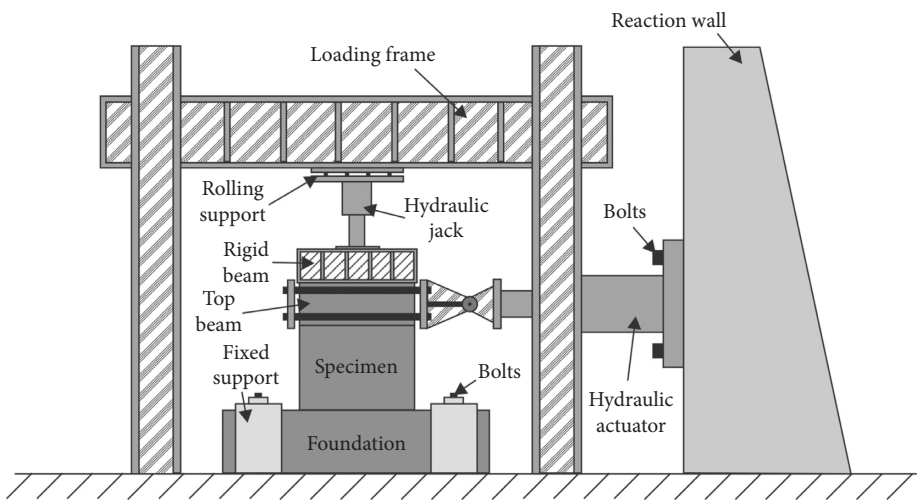

Figure 2: Test setup.

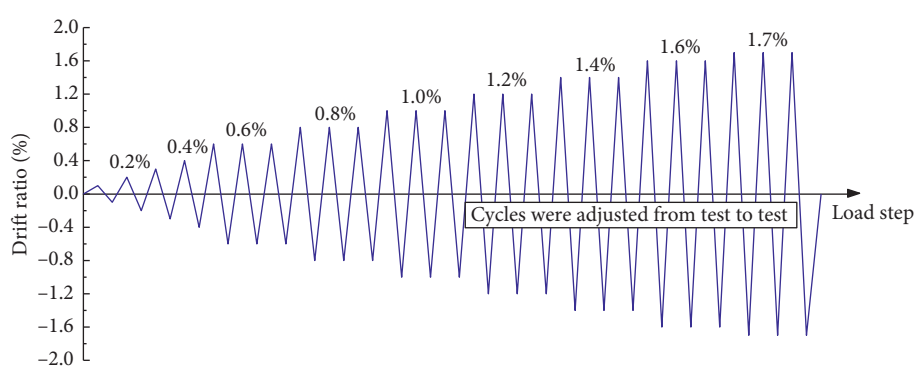

Figure 3: Loading history.

locations. The horizontal LVDT of L1 was arranged longitudinally along the wall to measure the lateral displacement. The horizontal LVDT of L2 monitored any slip of the foundation beams. The diagonal LVDTs L3 and L4 were set to measure the shear deformation. In addition, the displacement of specimens under different load levels was measured by the vertical LVDTs L5 and L6, which were mounted at the base of walls.

Moreover, nine strain gauges were arranged along the diagonal line on the steel plate, five strain gauges were arranged on the bottom of that, and eight strain gauges were arranged on both sides of that, to record its strain development. The arrangements of displacement transducers and strain gauges are shown in Figure 4. The failure process could be carefully observed and manually recorded during the tests. The axial compressive ratio n was calculated from the following equation:

$$n = \frac{N}{f_y A_s + f_c A_c}, \quad (1)$$

where N denotes the axial compression load; f_y denotes the yield strength of the steel plate; f_c denotes the prism compressive strength of the concrete; and A_c and A_s denote the cross-sectional areas of the concrete wall and steel plates, respectively.

3. Test Results and Analysis

3.1. Failure Process and Mode of Test Specimens. The failure modes of the three DSC composite shear walls with low shear-to-span ratio under combined action of axial compression load and cycle horizontal force are shown in Figure 5. Similar damage patterns of local buckling of steel plates and compressive crushing of concrete were observed in the wall specimens. Currently, three stages were used to describe the damage process. At the elastic state, the steel plate at the both boundary element of composite walls had no visual evidence of local buckling. As the drift ratios were up to 0.5%, the composite walls were yielded. At 0.6% drift, the stiffness of load-displacement curves began to decrease with the displacement increasing sequentially. When the composite walls were in the damage developing stage, the slight local buckling sustaining was observed in the boundary element at the base of the wall. The local buckling became more noticeable with the increase of loading. When the drift reached 1.0%, the steel plates buckling was observed from wall web. And it was the failure stage after it reached to the maximum load. At 1.2% drift, the specimen reached maximum load. The vertical fracture developed along the weld of the bottom from the DSC composite walls. It was shown that the vertical fracture developed along the weld of the bottom from the DSC composite walls. The steel plate was fractured along the weld in vertical under the influence of large plastic transverse strain, which is caused by the transverse expansion of the compressed filled concrete. Concrete was immediately crushed as soon as the steel fractured. Then, the wall specimens were destroyed completely, and the capacity of vertical load carrying was lost at further cycles. The damage of concrete at the bottom of wall aggravated with the increase of axial compressive ratio. With the increase of steel ratio, the local bucking of steel plate is delayed effectively, and the deformation capacity is improved.

3.2. Lateral Load-Displacement Relationship. Figure 6 presents the lateral load-displacement relationship for the composite walls. The hysteresis loops were not plump with pinching behavior, but not loss of stiffness at drift ratios greater than 1%. Before the steel plate yielded, the hysteresis curves of all composite walls almost developed linearly. Then, a steady decrease of the loading stiffness occurred as the lateral load increased. And the residual deformation was more prominent after the maximum load. As the steel ratio increased, the width of hysteresis loops increased. DSCW-2 was wider than DSCW-1. The hysteresis loops of specimens with lower axial compression ratio were obviously wider. As the steel plate formed a cavity cross section, the concrete was restrained effectively. It indicated that there was significant improvement for the hysteresis behavior of the DSC composite wall. A plateau can be observed in the hysteretic response of the walls, which shows that steel plate helps maintain peak load for cycles at displacements beyond maximum load. According to the load-displacement hysteresis curves, three specimens' skeleton curves are shown. The axial compression ratio of DSCW-1 and DSCW-2 is the same, but the steel ratio of DSCW-2 is larger. Therefore, the skeleton curve of DSCW-2 descends slightly, and its post-yielding deformation capacity is better. The specimen of DSCW-3 had the high axial compression ratio; therefore, the descending branch of the load-deformation curve becomes shorter, which shows that the ductility of the structural wall is poor.

3.3. Lateral Load Resisting Capacity. Table 2 showed the loads at characteristic points of the four specimens, where V_y and V_m are the corresponding yielding load and maximum load, respectively. The load at the yielding point was determined with the equivalent elastic-plastic yielding-based method, which is described in Figure 7. The axial compression load for DSCW-3 is greater than that for DSCW-2; therefore, the yielding loads and the maximum load of DSCW-3 are higher. In regard to the variation of steel ratio, the composite walls with higher steel ratio show higher lateral load resisting capacity. Compared to DSCW-1, the lateral load resisting capacity of DSCW-2 was improved to 12.7% and that of DSCW-3 improved by 7.8% compared to DSCW-2. The value of V_m/V_y, for the three shear wall specimens is between 1.29 and 1.33, which indicates that the load-bearing capacity of the specimens is of a reasonable margin after yielding.

3.4. Deformation Capacity. The yield displacement (Δ_y) and ultimate displacement (Δ_u) obtained are listed in Table 3. The yield displacements corresponded to the yield load. The ultimate displacement corresponded to displacement when the

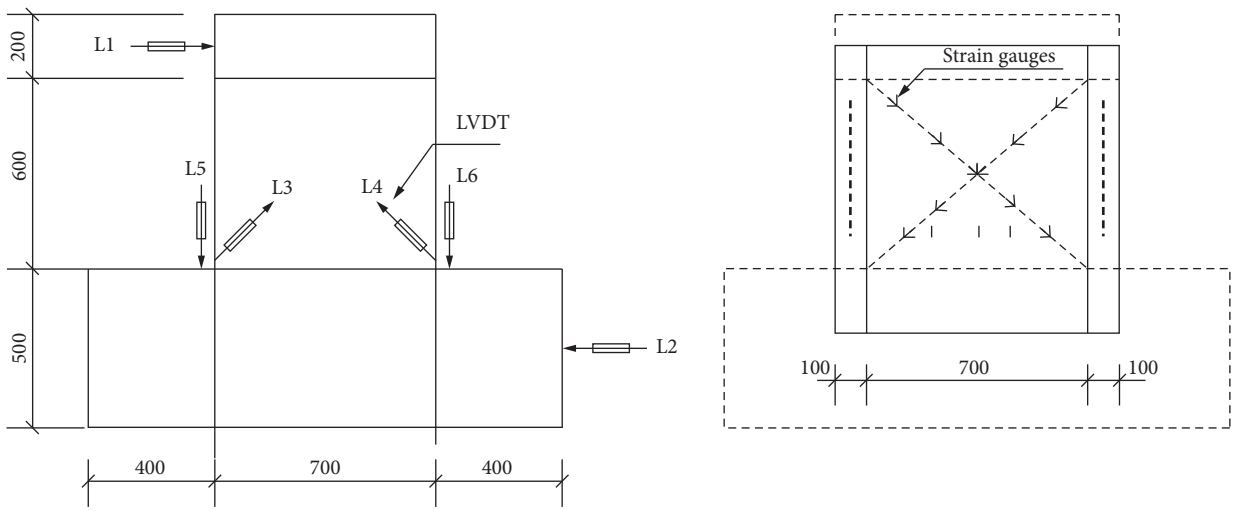

Figure 4: Displacement transducers arrangement.

(a) (b) (c)

Figure 5: Failure model. (a) DSCW-1. (b) DSCW-2. (c) DSCW-3.

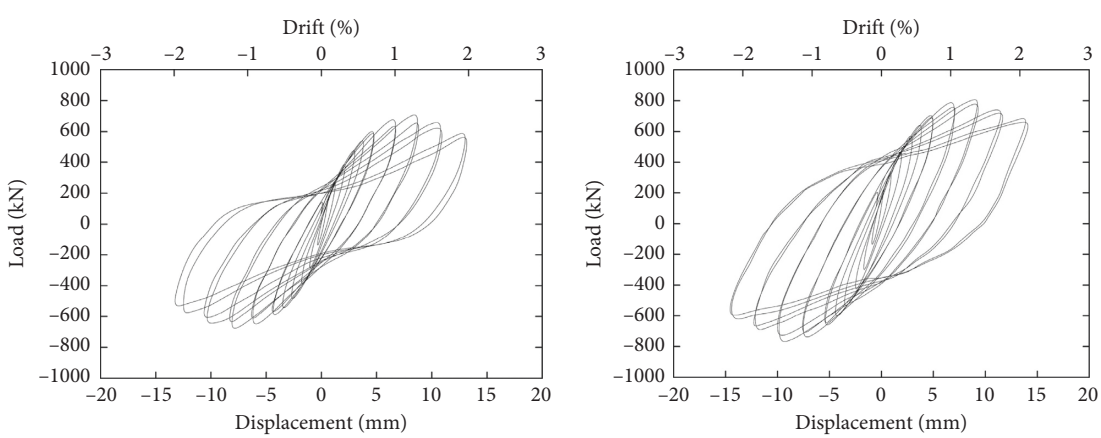

(a) (b)

Figure 6: Continued.

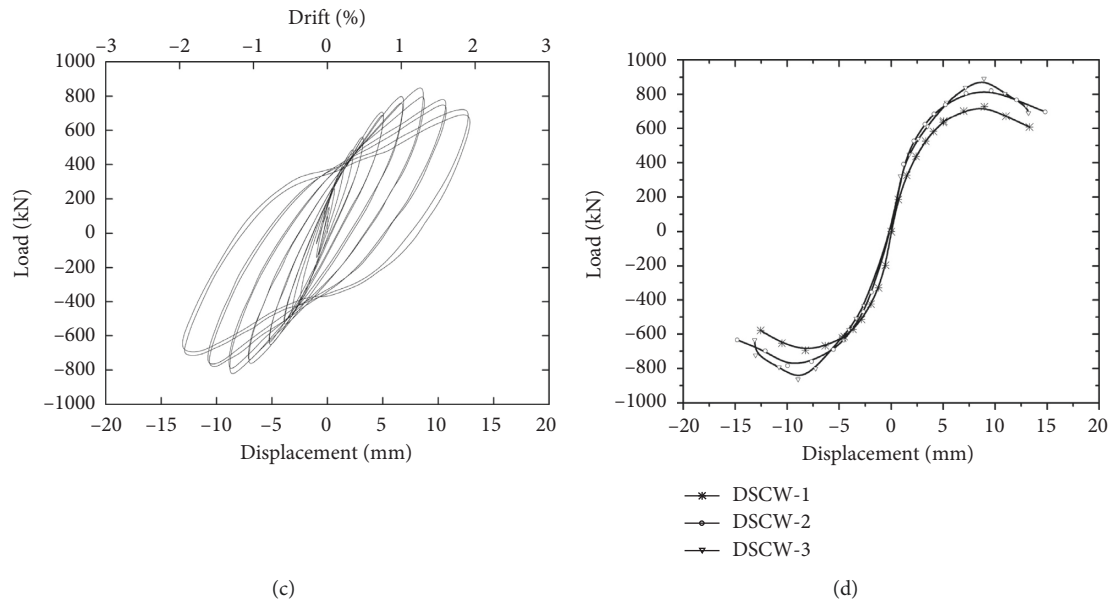

Figure 6: Lateral load versus top displacement relationship. (a) DSCW-1. (b) DSCW-2. (c) DSCW-3. (d) Envelope curves.

Table 2: Lateral load resisting capacity.

Specimens	V_y/kN	V_m/kN	V_m/V_y
DSCW-1	536.3	711.2	1.33
DSCW-2	620.1	801.3	1.29
DSCW-3	655.2	863.6	1.32

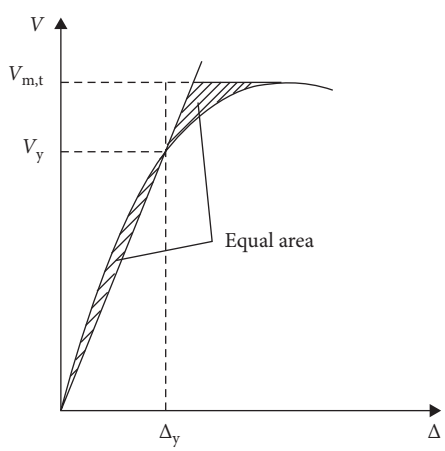

Figure 7: Determination method of yield displacement.

Table 3: Lateral displacement and ductility coefficient.

Specimens	Δ_y/mm	Δ_u/mm	μ	θ
DSCW-1	4.2	12.8	3.04	1/55
DSCW-2	4.6	14.7	3.30	1/46
DSCW-3	4.3	12.5	2.76	1/55

load decreased to 85% of the maximum lateral load. The ductility coefficients (μ) were calculated as Δ_y/Δ_u, and the ultimate drift ratios (θ) were calculated as Δ_u/H. The equivalent elastic-plastic yielding-based method is used to determine the yielding point. The specimens with the difference steel ratio showed similar deflection behavior. As the steel ratio increased, the yield displacement and the ultimate displacement increased; under the same steel ratio, the displacement of specimen DSCW-3 at yield displacement, ultimate displacement, and ductility coefficients decreased 7.0%, 17.6%, and 19.6% compared to DSCW-2, respectively. The steel ratio should not be less than 10%. In order to improve the comprehensive seismic performance of DSC composite walls, the method of increasing steel ratio with an acceptable price was exploited, which is effective and easy. The ductility coefficient of DSC composite wall can easily reach to 3.0.

3.5. Energy Dissipation Capacity. The energy dissipation capacity was calculated by the area enclosed under the lateral load (V) versus horizontal displacement (Δ) loop by each specimen during a cycle. The cumulative energy dissipation values of the three DSC composite wall specimens with under reversed cyclic lateral loading are shown in Figure 8. With the increase of load cycles, the area of hysteresis loops gradually increases after yielding. As the steel ratio increases, the energy dissipation of structural walls decreases gradually and the total energy dissipation of DSCW-2 is 27.2% more than that of DSCW-1. The energy dissipation capacity of DSCW-3 is less (21.6%) than that of DSCW-2 with the increase of the axial compression ratio.

The energy dissipation ability can also be evaluated by the equivalent viscous damping coefficients h_e. It is defined as (Figure 9)

$$h_e = \frac{1}{2\pi}\frac{S_{ABCDA}}{S_{OBE} + S_{ODF}}, \tag{2}$$

where S_{ABCDA}, S_{OBE}, and S_{ODF} are the area bounded by corresponding point.

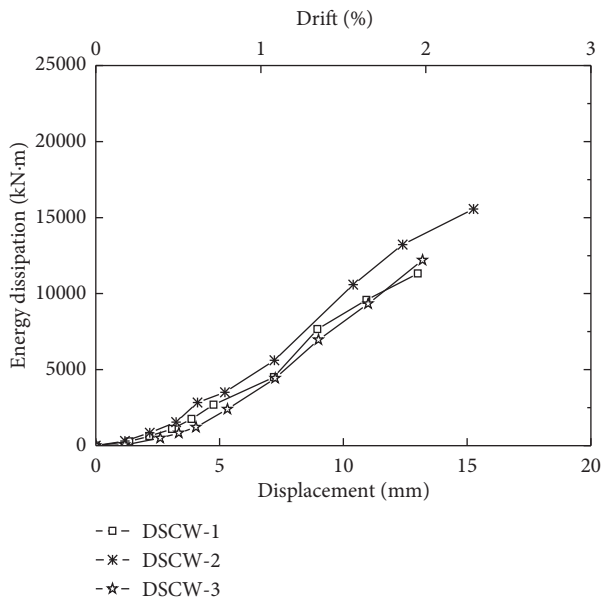

Figure 8: Energy dissipation curves.

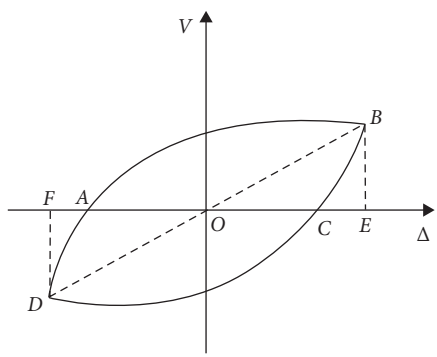

Figure 9: Calculation of equivalent viscous coefficient.

The equivalent viscous damping coefficients are shown in Table 4.

3.6. Stiffness Degradation. With the increase of cyclic lateral load and displacement, the plastic deformation developed continuously, and the stiffness gradually degenerated. The secant stiffness was used to show characteristics of the stiffness degradation of the specimens. The stiffness degradation of specimens was shown in Figure 10. The stiffness degradation ratio was the relative reduction compared with the initial stiffness. DSCW-1 had the highest degree of stiffness degradation while DSCW-2 owned the lowest degree of stiffness degradation.

The stiffness degradation decreased with increasing the steel ratio; the stiffness declined more quickly as the composite walls increased axial compression ratio. It can be seen from Figure 10 that the stiffness degradation process can be divided into three phases: the fast descending phase from the initial to the yielding; the medium-speed descending phase from yielding to maximum lateral load; and the slow descending phase from maximum load to ultimate deformation.

Table 4: Equivalent viscous damping coefficient.

Dissipative coefficient h_e	DSCW-1	DSCW-2	DSCW-3
	0.196	0.249	0.238

3.7. Strain Analysis. The maximum strains were located at the edges of the wall base section. The hysteresis loops formed by lateral load and vertical strains of steel plate in specimen DSCW-2 are shown in Figures 11(a) and 11(b), whose strain is similar to that of other specimens. Because of the constant axial compressive forces, the steel plates first yielded in compression. Due to the effect of the steel buckling and concrete crushing at the bottom of the wall, the increase rate of compressive strains is clearly greater than that of tensile strains at large drifts cycles. The maximum compressive and tensile strains are different at the peak load and the ultimate displacement.

4. Numerical Simulation

Nonlinear finite element analysis (FEA) can be implemented effectively, in order to predict the structural behavior as realistically as possible. Three-dimensional (3-D) finite element analysis (FEA) is considered to examine previously tested and analyzed under cyclic loading DSC composite walls using the FEA software ABAQUS [20]. The selection of this software is based on its availability and its well-recognized capabilities in modelling the behavior of steel and concrete structures. The adopted FEA model is used to analyze and investigate the failure modes and loads of the DSC composite walls.

4.1. Material Modelling. The tension test was conducted to define stress-strain relationship of the steel plate. Figure 12(a) shows the steel plate with the thickness of 3 mm. The idealized elastic-plastic model was considered to simulate constraining bolt and stud in Figure 12(b), and the hardening modulus was defined as $E_s' = 0.01E_s$. The yield and ultimate strengths of constraining bolt and stud were 381 MPa to 529 MPa and 438 MPa to 545 MPa, respectively. The elastic modulus was 2.06×10^5 N/mm^2. Poisson's ratio was taken as 0.3.

The theory, which assumed the steel to have bilinear kinematic hardening behavior, is adopted to explain the progression of hardening and softening effects. The content of the theory is as follows: (1) the equivalent stress was unconsidered during the yielding of the steel and (2) the Bauschinger effect [21] is taken into consideration. In order to make the simulation results be closer to realistic behavior, the parameters of compression strength, strains, and elastic modulus were obtained from the concrete compressive test. The concrete damage plastic model (CPDM) offered in ABAQUS is adopted for modelling the concrete. The CPDM introduced the damage index into the concrete model and reduced the elastic stiffness matrix of the concrete. Tensile cracking and compression crushing of concrete were considered in CPDM. The equations developed by the Chinese Code (GB50010-2010) [22] were implemented in the compression and tension stress-strain relationships of concrete. The relationships are shown in Figure 13. The

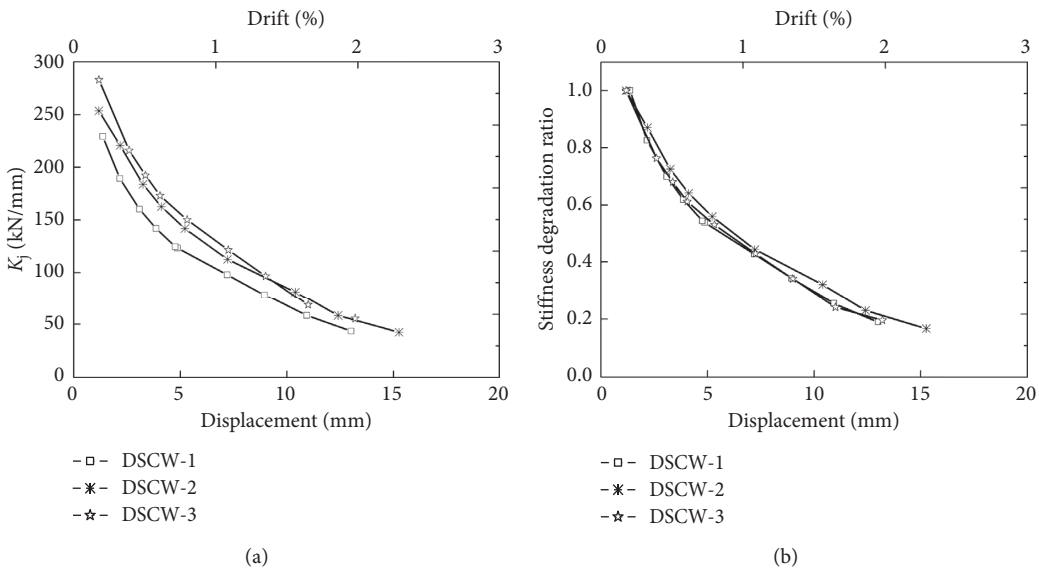

Figure 10: Stiffness degradation of specimens. (a) Stiffness degradation curves. (b) Stiffness degradation ratio curves.

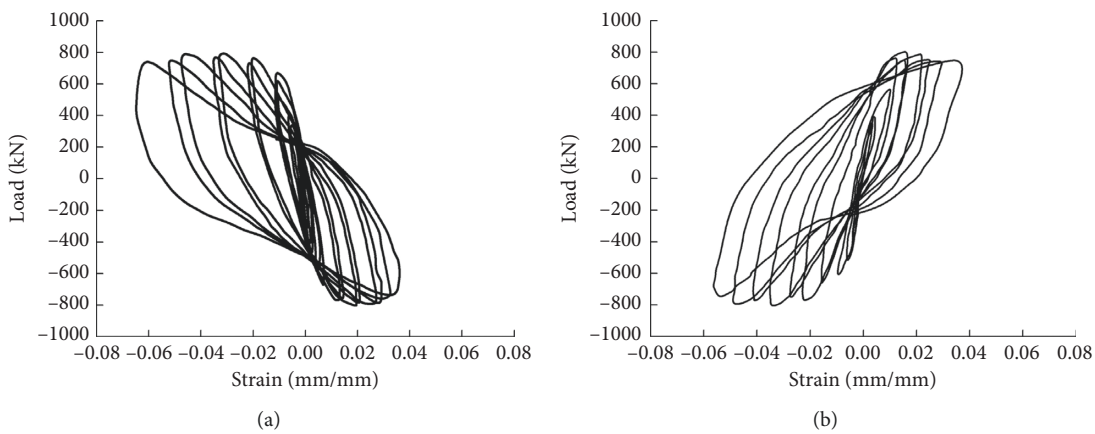

Figure 11: Strain of specimens. (a) Left edge strain. (b) Right edge strain.

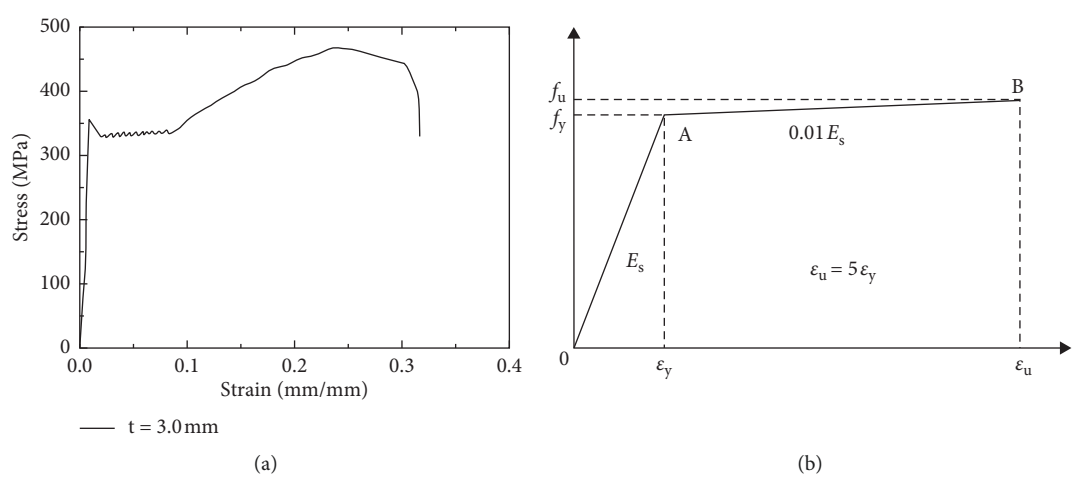

Figure 12: (a) Stress-strain of steel plate. (b) Stress-strain of constraining bolt and stud.

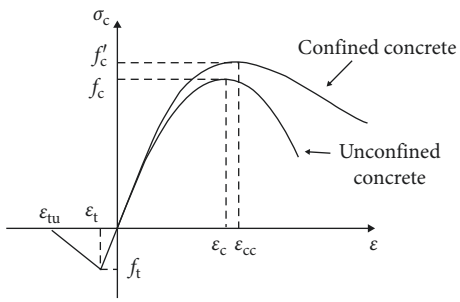

Figure 13: Stress-strain of concrete.

damage index was considered in the equation. The strain-stress equations of compression and tension are as follows:

$$
\begin{aligned}
\sigma &= (1-d_c)E_c\varepsilon,\\
d_c &= \begin{cases} 1-\dfrac{\rho_c n}{n-1+x^n}, & x \le 1,\\[2ex] 1-\dfrac{\rho_c}{\alpha_c(x-1)^2+x}, & x > 1,\end{cases}\\
\rho_c &= \frac{f_c}{E_c\varepsilon_c},\\
n &= \frac{E_c\varepsilon_c}{E_c\varepsilon_c - f_c},\\
\varepsilon_c &= \left(700 = 172\sqrt{f_c}\right)\times 10^{-6},\\
\alpha_c &= 0.157 f_c^{0.785} - 0.905,\\
\sigma &= (1-d_t)E_c\varepsilon,\\
d_t &= \begin{cases} 1-\rho_t\left[1.2-0.2x^5\right], & x \le 1,\\[2ex] 1-\dfrac{\rho_t}{\alpha_t(x-1)^{1.7}+x}, & x > 1,\end{cases}\\
\rho_t &= \frac{f_c}{E_c\varepsilon_c},\\
\varepsilon_t &= f_t^{0.54}\times 65\times 10^{-6},\\
\alpha_t &= 0.312 f_t^2,
\end{aligned}
\tag{3}
$$

where $x = \varepsilon/\varepsilon_c$ and $y = \sigma/f_c$; σ and ε denote stress and strain of concrete, respectively; d_c and d_t denote the compression damage parameter and tension damage parameter, respectively; ε_c denotes the compression strain corresponding to f_c; and ε_t denotes the tension strain corresponding to f_y. Poisson's ratio of concrete was taken as 0.2.

The confined concrete constitutive model [23] was used to take into account the steel plate constraint on concrete. The stress-strain relationships are shown in Figure 13. The equations are expressed as follows:

$$
\begin{aligned}
y &= \begin{cases} 2x - x^2, & (x \le 1),\\[2ex] \dfrac{x}{\beta(x-1)^\eta + x}, & (x > 1),\end{cases}\\
\varepsilon_{cc} &= \left(1300 + 12.5 f'_c + 800\xi^{0.2}\right)\times 10^{-6},\\
\xi_0 &= \frac{A_s f_y}{A_c f_c},\\
\beta &= \frac{(f'_c)^{0.1}}{\left(1.2(1+\xi_0)^{0.5}\right)},\\
\eta &= 1.6 + 1.5x,
\end{aligned}
\tag{4}
$$

where $x = \varepsilon/\varepsilon_{cc}$ and $y = \sigma/f'_c$; σ_c and ε are the concrete stress and strain, respectively; ε_{cc} denotes the compression strain corresponding to σ_0; and ξ_0 denotes the confinement factor.

4.2. Element Contact Properties and Boundary Conditions. The concrete was modelled with three-dimensional 8-node solid elements (C3D8R). The buckling behavior was considered for the steel plate which was modelled with S4R element. The T3d2 element was modelled for constraining bolt and stud. As the steel plate was connected to concrete surfaces directly in the test setup, it is necessary to develop the reasonable contact analysis. The surface-to-surface contact was adopted to simulate interaction between the steel plate and concrete, which was defined by using the "penalty algorithm option." All nodes at the bottom of the basic beam were specified by restraining the six degrees of freedom. It is consistent with the characteristics of the prototype. The vertical load was applied to the top beam in the uniform distribution. Moreover, to prevent undesirable local buckling at the top of the model, the lateral load was exerted on the models by defining a reference point. Finite element (FE) analysis model of DSCW-3 is shown in Figure 14. To consider the cyclic behavior of the composite wall, the displacement control mode was adopted as the load method. During the loading process, the displacement increases step-by-step until the model reaches ultimate deformation capacity. A mesh size of approximately 28 elements along the wall length was targeted based on a sensitive analysis discussed. Furthermore, it is not allowed to separate the surfaces of the two bodies for the purpose of overcoming the problems of convergence and making the computational time optimized.

4.3. Comparison of Experimental and Analytical Results. The FE analysis models were able to simulate the experimental loading process. As shown in Figure 15 and Table 5, the experimental result was in the boundary of the numerically simulated curve, which has a good effect on extrusion and softening properties. However, the results of finite element analysis, under load reversal, showed that the cyclic loop had softening mechanism and pinching phenomenon. The

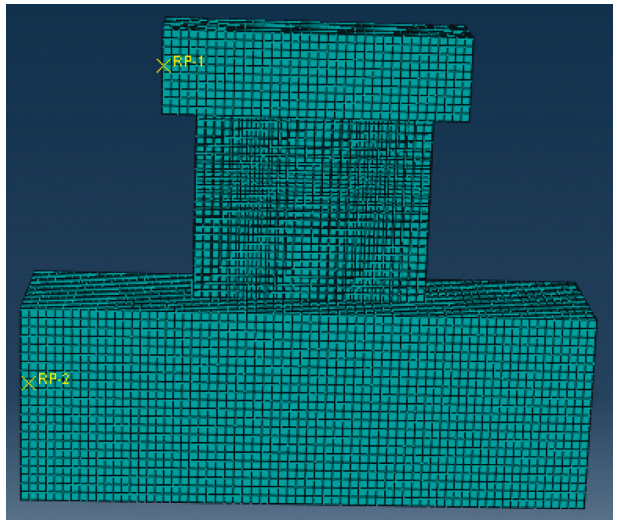

Figure 14: FE model of DSCW-3.

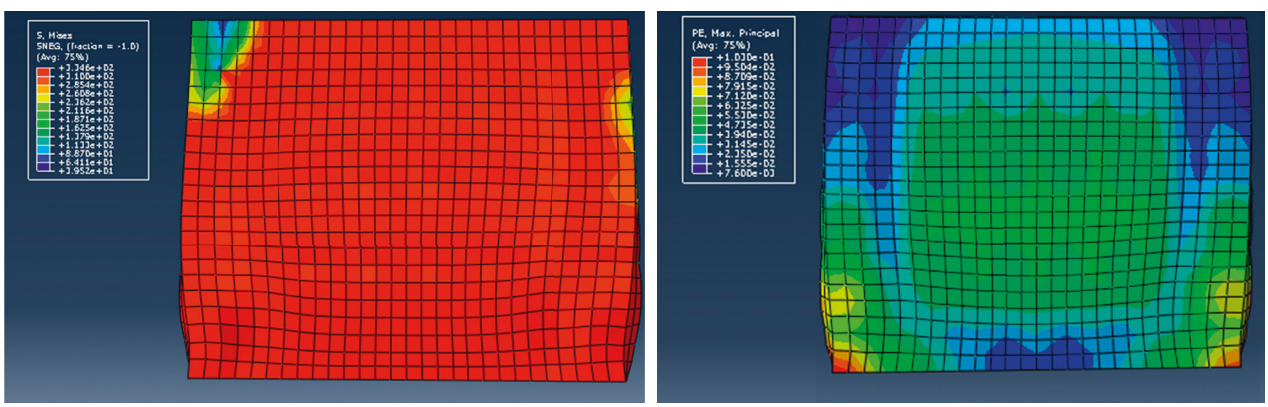

Figure 15: Stress and strain in composite walls.

Table 5: Lateral load resisting capacity and displacement of FE specimens.

Specimens	$V_{m,FE}$/KN	$\Delta_{u,FE}$/mm	$V_{m,FE}/V_m$
DSCW-1	715.2	13.2	1.01
DSCW-2	787.3	14.5	0.98
DSCW-3	830.6	12.8	0.97

hysteretic curves of FE models were plumper than that of test specimens, and the load-carrying capacity subsequently decreased slowly after the maximum load. The initial stiffness of the FE curves was slightly higher than the experimental curves, but it is still acceptable. The reason might be mainly attributed to material properties from the factual properties and the bond behavior between steel plate and concrete. The FE models of composite walls underestimated the actual lateral load-carrying capacity. Numerical FE curve of DSCW-1 was closest to the experimental curve. For the composite walls, the lateral load resisting capacity obtained by FE models is 101%, 98%, and 97% corresponding to DSCW-1, DSCW-2, and DSCW-3. These overestimations may have occurred because of the constitutive relations of unconfident concrete and FE analysis for buckling of steel plate. The stress results of steel plate and maximum principal tensile plastic strain from the finite element analyses are shown in Figure 16. It was observed that the largest stress and steel plate buckling and the crushing and spalling of the infill concrete concentrations occurred at the end of the DSC composite wall base. The postbuckling of steel plate was observed from FE analysis as similar to experimental results.

5. Conclusions

The seismic behavior of double steel concrete composite shear walls was studied in this paper. Three DSC composite walls with an aspect ratio of 1.0 were tested under quasistatic loading. The seismic behavior of DSC composite walls was investigated. Numerical analysis, using nonlinear FE software ABAQUS, was performed. Based on the results, the following observations and conclusions were drawn:

(1) The typical failure modes of DSC composite wall were steel plate local buckling and concrete failure at the bases of composite walls. The steel plate and concrete had a reliable connection with studs.

(2) The DSC composite walls were not plump with pinching, high lateral load resisting capacity, and relatively slow degradation of stiffness. The ductility

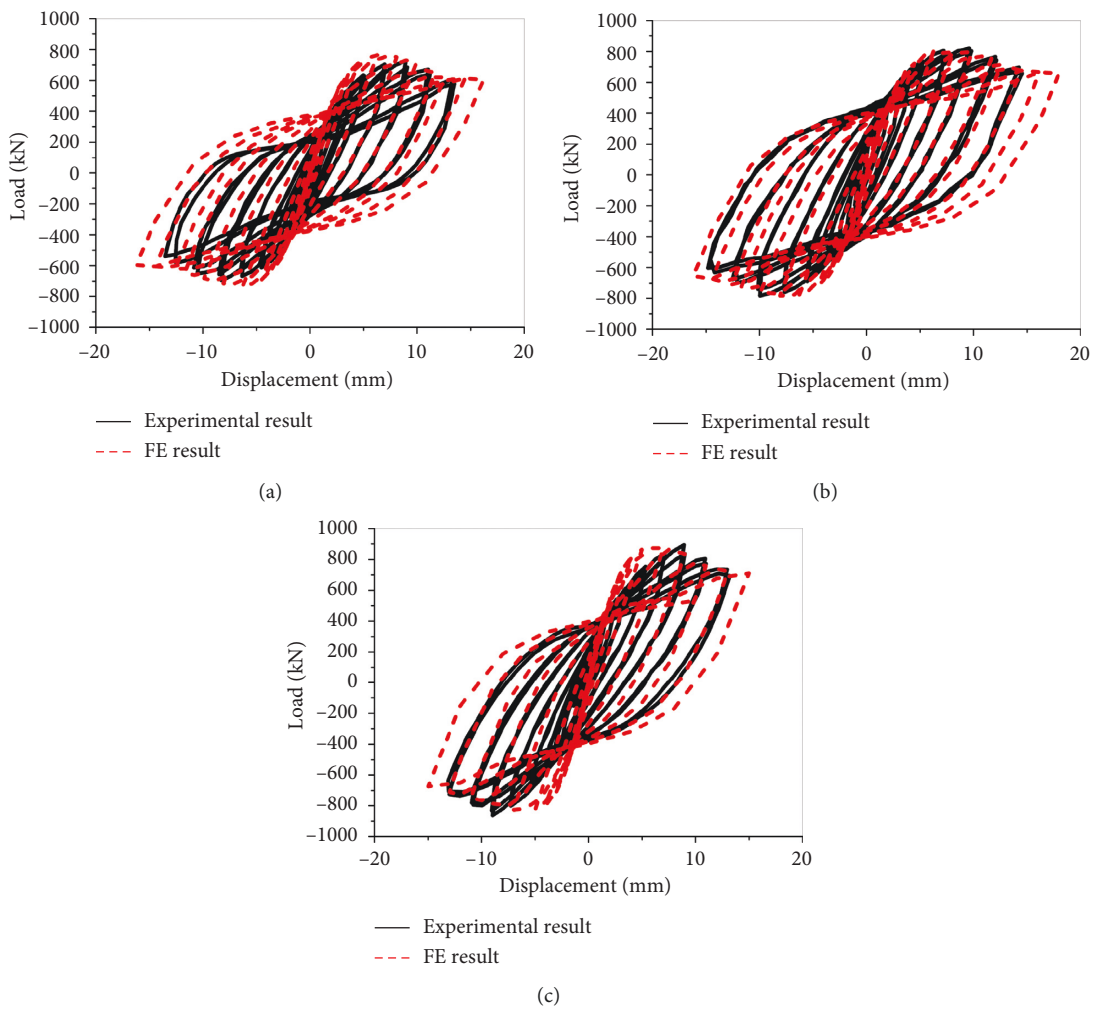

Figure 16: Comparison between experimental results and FE results. (a) DSCW-1. (b) DSCW-2. (c) DSCW-3.

coefficient ranged from 2.76 to 3.30, which increased with steel ratio and decreased with axial compression ratio. The energy dissipation capacity of the specimens was improved with the increase of steel ratio at the same axial compression ratio. The DSC composite walls with effective confinement boundary elements could resist large lateral load resisting capacity and show good ductility.

(3) The FE models were able to simulate the failure process of the double steel concrete composite walls. The bilinear kinematic hardening behavior of steel plate was considered. The damage progress of concrete was simulated with the concrete damage plastic model (CPDM). The steel plate buckling concentrations occurred at the base of DSC composite wall. The results of FE analysis and test are in good agreement.

Data Availability

The data used to support the findings of this study are available from the corresponding author upon request.

Conflicts of Interest

The authors declare that they have no conflicts of interest.

Acknowledgments

The help and support received from the laboratory staff of Structural Engineering, Civil Engineering School, Chang'an University, is greatly appreciated. This research was financially supported by the National Natural Science Foundation of China (grant no. 51308052), Natural Science Foundation of Shanxi Province (grant no. 2017JM037), and Fundamental Research Funds for the Central Universities. The financial support was gratefully acknowledged.

References

[1] P. A. Hidalgo, C. A. Ledezma, and R. M. Jordan, "Seismic behavior of squat reinforced concrete shear walls," *Earthquake Spectra*, vol. 18, no. 2, pp. 287–308, 2002.

[2] I. Ricci, M. Palermo, G. Gasparini, S. Silvestri, and T. Trombetti, "Results of pseudo-static tests with cyclic

horizontal load on cast in situ sandwich squat concrete walls," *Engineering Structures*, vol. 54, no. 9, pp. 131–149, 2013.

[3] R. A. Link and A. E. Elwi, "Composite concrete-steel plate walls: analysis and behavior," *Journal of Structural Engineering*, vol. 121, no. 4, pp. 260–267, 1995.

[4] M. Ozaki, S. Akita, H. Osuga, T. Nakayama, and N. Adachi, "Study on steel plate reinforced concrete panels subjected to cyclic in-plane shear," *Nuclear Engineering and Design*, vol. 228, no. 1-3, pp. 225–244, 2004.

[5] P. Prabha, V. Marimuthu, M. Saravanan, G. S. Palani, N. Lakshmanan, and R. Senthil, "Effect of confinement on steel-concrete composite light-weight load-bearing wall panels under compression," *Journal of Constructional Steel Research*, vol. 81, no. 2, pp. 11–19, 2013.

[6] K. Zhang, A. H. Varma, S. R. Malushte, and S. Gallocher, "Effect of shear connectors on local buckling and composite action in steel concrete composite walls," *Nuclear Engineering and Design*, vol. 269, no. 10, pp. 231–239, 2014.

[7] H.-S. Hu, J.-G. Nie, and M. R. Eatherton, "Deformation capacity of concrete-filled steel plate composite shear walls," *Journal of Constructional Steel Research*, vol. 103, pp. 148–158, 2014.

[8] K. Emori, "Compressive and shear strength of concrete filled steel box wall," *Steel Structures*, vol. 26, no. 2, pp. 29–40, 2002.

[9] S. K. Clubley, S. S. J. Moy, and R. Y. Xiao, "Shear strength of steel-concrete-steel composite panels. Part I-testing and numerical modelling," *Journal of Constructional Steel Research*, vol. 59, no. 6, pp. 781–794, 2003.

[10] S. K. Clubley, S. S. J. Moy, and R. Y. Xiao, "Shear strength of steel-concrete-steel composite panels. Part II-detailed numerical modelling of performance," *Journal of Constructional Steel Research*, vol. 59, no. 6, pp. 795–808, 2003.

[11] K. M. A. Hossain and H. D. Wright, "Flexural and shear behaviour of profiled double skin composite elements," *Steel and Composite Structures*, vol. 4, no. 2, pp. 113–132, 2004.

[12] K. M. A. Hossain and H. D. Wright, "Behaviour of composite walls under monotonic and cyclic shear loading," *Structural Engineering and Mechanics*, vol. 17, no. 1, pp. 69–85, 2004.

[13] T.-S. Eom, H.-G. Park, C.-H. Lee, J.-H. Kim, and I.-H. Chang, "Behavior of double skin composite wall subjected to in-plane cyclic loading," *Journal of Structural Engineering*, vol. 135, no. 10, pp. 1239–1249, 2009.

[14] J.-G. Nie, H.-S. Hu, J.-S. Fan, M.-X. Tao, S.-Y. Liu, and F.-J. Liu, "Experimental study on seismic behavior of high-strength concrete filled double-steel-plate composite walls," *Journal of Constructional Steel Research*, vol. 88, no. 9, pp. 206–219, 2013.

[15] X. Ji, F. Jiang, and J. Qian, "Seismic behavior of steel tube-double steel plate-concrete composite walls: experimental tests," *Journal of Constructional Steel Research*, vol. 86, no. 4, pp. 17–30, 2013.

[16] L. Chen, H. Mahmoud, S.-M. Tong, and Y. Zhou, "Seismic behavior of double steel plate-HSC composite walls," *Engineering Structures*, vol. 102, no. 11, pp. 1–12, 2015.

[17] Y. Zhou and M. Bruneau, "In-Plane cyclic testing of concrete-filled sandwich steel panel walls with and without boundary elements," *Journal of Structural Engineering*, vol. 143, no. 9, pp. 1–12, 2017.

[18] E. Siamak, S. W. Andrew, H. V. Amit et al., "Finite element modeling of steel-plate concrete composite wall piers," *Engineering Structures*, vol. 101, no. 7, pp. 246–263, 2015.

[19] E. Polat and M. Bruneau, "Modeling cyclic inelastic in-plane flexural behavior of concrete filled sandwich steel panel walls," *Engineering Structures*, vol. 148, no. 10, pp. 63–80, 2018.

[20] K. Hibbit and Sorensen, *Abaqus 6.11 Online Documentation., Abaqus Analysis User's Manual,*Dassault Systems Inc, Johnston, RI, USA, 2011.

[21] R. G. Driver, G. L. Kulak, A. E. Elwi, and D. J. L. Kennedy, "FE and simplified models of steel plate shear wall," *Journal of Structural Engineering*, vol. 124, no. 2, pp. 121–130, 1998.

[22] Kennedy, *Code for Seismic Design of Buildings. GB 50011-2010*, Ministry of Housing and Urban-Rural Development of the People's Republic of China, Beijing, China, 2010, in Chinese.

[23] L. H. Huang and Z. Tao, "Performance of concrete-filled thin-walled steel tubes under pure torsion," *Thin-Walled Structures*, vol. 45, no. 2, pp. 24–36, 2007.